Conformational Transitions in Potential and Free Energy Space for Furanoses and 2′-Deoxynucleosides

Henry A. Gabb and Stephen C. Harvey*

Contribution from the Department of Biochemistry, University of Alabama at Birmingham, Schools of Medicine and Dentistry, Birmingham, Alabama 35294-0005

Received November 20, 1992

Abstract: A comprehensive molecular modeling study of the four commonly occurring 2′-deoxynucleosides (dN's) was carried out to determine whether pseudorotation phase angle (P), N-glycosidic torsion (χ), and pucker amplitude (ν_m) are energetically coupled. To this end, the AMBER all-atom force field (Weiner et al. *J. Comput. Chem.* **1986**, *7*, 230) was rigorously parametrized for ribose and 2′-deoxyribose to best fit existing data using both energy minimization and molecular dynamics (MD). Twenty 300 K, 1-ns in vacuo MD simulations were carried out for each dN to sample thermodynamically accessible regions of conformational space. This data was used to construct potential of mean force surfaces, PMF(P,χ). Adiabatic mapping was used to generate potential energy surfaces, $V(P,\chi)$, for each dN. We also used two newer methods to examine conformational transitions in dN's. Specifically, we used the Ulitsky and Elber algorithm (*J. Chem. Phys.* **1990**, *92*, 1510) and the CONTRA MD algorithm developed in this laboratory to determine the preferred pathway, both $V(P,\chi)$ and PMF(P,χ), for the C2′-endo/anti to C3′-endo/syn transition. Our results suggest that the P and χ transitions are not energetically coupled in the most plausible pathways from C2′-endo/anti to C3′-endo/syn. Finally, $\nu_m(P)$ is also examined in both potential and free energy hyperspace. We conclude that ν_m contributes entropically to furanose flexibility in a manner not readily apparent using only potential energy calculations.

Introduction

The local structure of 2′-deoxynucleosides (dN's) is a determining factor in nucleic acid structure. The three major DNA conformations (i.e. A, B, and Z) can be defined by the pseudorotation phase (P) and N-glycosidic torsion (χ) angles of their dN residues.[1] For example, nucleotide residues in B-DNA are C2′-endo while those of A-DNA are in the C3′-endo pucker mode. In Z-DNA, purine residues adopt the C3′-endo configuration and pyrimidines adopt the C2′-endo one. So, conformational transitions between these three families are always accompanied by changes in P and sometimes by changes in χ (e.g. purine residues in the B- to Z-DNA transition). Presently, it is difficult to generate thermodynamic ensembles for oligonucleotides using molecular dynamics (MD). For this reason, we opted to model free dN's using long MD simulations in order to sample all thermodynamically accessible regions of conformational space for these building blocks of oligonucleotides.

For a furanose ring to be planar, all of its torsion angles must be cis. Since this is a high-energy state, cyclic sugar molecules pucker to relieve torsional stress. The concept of pseudorotation is used to precisely describe the furanose puckering phase angle by the following formula

$$P = \arctan\left[\frac{(\nu_4 + \nu_1) - (\nu_3 + \nu_0)}{2\nu_2(\sin 36° + \sin 72°)}\right] \quad (1)$$

where the ν_i are the five endocyclic torsion angles.[2,3] The IUPAC definitions for the endocyclic torsions are ν_0, C4′–O4′–C1′–C2′; ν_1, O4′–C1′–C2′–C3′; ν_2, C1′–C2′–C3′–C4′; ν_3, C2′–C3′–C4′–O4′; and ν_4, C3′–C4′–O4′–C1′. For any phase angle, P, $\nu_0 + \nu_1 + \nu_2 + \nu_3 + \nu_4 = 0$. Pucker amplitude, ν_m, or the maximum deviation of any torsion angle from zero, is calculated for the Altona and Sundaralingam[3] description as follows

$$\nu_m = \frac{\nu_2}{\cos P} \quad (2)$$

This method, however, does not treat all endocyclic torsions equally (i.e. ν_2 is the reference torsion for eqs 1 and 2). So, ν_m is dependent on the position of O4′ (i.e. the atom opposite ν_2). The Fourier sum method of Rao et al.[4] treats all endocyclic torsions equally so pucker amplitude and phase are no longer coupled variables.

$$A = \frac{2}{5}\sum_{j=0}^{4}\nu_j\left(\frac{4\pi j}{5}\right)$$

$$B = -\frac{2}{5}\sum_{j=0}^{4}\nu_j\left(\frac{4\pi j}{5}\right)$$

$$\nu_m = (A^2 + B^2)^{1/2} \quad (3)$$

$$P = \arctan\left(\frac{B}{A}\right) \quad (4)$$

In both methods, the phase angle $P = 0°$ (N) is the C2′-exo–C3′-endo pucker and $P = 180°$ (S) is the C2′-endo–C3′-exo pucker. For a comparison of commonly used methods for calculating P and ν_m, see ref 5.

Crystallographic,[3,6-8] solution,[9,12] and theoretical[5,13-16] studies all agree that the furanose ring in ribose, 2′-deoxyribose, and

* Corresponding author: tel, 205-934-5028; e-mail, harvey@neptune.cmc.uab.edu.

(1) Dickerson, R. E. *Methods Enzymol.* **1992**, *211A*, 67–111.
(2) Altona, C.; Geise, H. J.; Romers, C. *Tetrahedron* **1968**, *24*, 13.
(3) Altona, C.; Sundaralingam, M. *J. Am. Chem. Soc.* **1972**, *94*, 8205–8212.
(4) Rao, S. T.; Westhof, E.; Sundaralingam, M. *Acta Crystallogr., Sect. A: Found. Crysallogr.* **1981**, *37*, 421–425.
(5) Harvey, S. C.; Prabhakaran, M. *J. Am. Chem. Soc.* **1986**, *108*, 6128–6136.
(6) de Leeuw, H. P. M.; Haasnoot, C. A. G.; Altona, C. *Isr. J. Chem.* **1980**, *20*, 108–126.
(7) Westhof, E.; Sundaralingam, M. *J. Am. Chem. Soc.* **1980**, *102*, 1493–1500.
(8) Pattabiraman, N.; Rao, M. J. *Int. J. Biol. Macromol.* **1982**, *4*, 91–98.
(9) Altona, C.; Sundaralingam, M. *J. Am. Chem. Soc.* **1973**, *95*, 2333–2344.
(10) Davis, D. B.; Danyluk, S. S. *Biochemistry* **1974**, *13*, 4417–4434.
(11) Davis, D. B.; Danyluk, S. S. *Biochemistry* **1975**, *14*, 543–554.
(12) Evans, F. E.; Sarma, R. H. *Nature* **1976**, *263*, 567–572.
(13) Olson, W. K. *J. Am. Chem. Soc.* **1982**, *104*, 278–286.
(14) Levitt, M.; Warshel, A. *J. Am. Chem. Soc.* **1978**, *100*, 2607–2613.

0002-7863/93/1515-4218$04.00/0

dN's is biphasic and flexible. Furanose rings show two preferred pucker modes centered around C2′- and C3′-endo. Ribose has a slight preference (~0.2 kcal/mol) for C3′-endo over C2′-endo.[13] The more asymmetric 2′-deoxyribose, however, shows a marked preference (~1.0 kcal/mol) for C2′-endo over C3′-endo.[6,13] This is due to the gauche effect.[13]

One theoretical study has reported that the barrier between C2′- and C3′-endo is as low as 0.5 kcal/mol for both ribose and 2′-deoxyribose.[14] This would mean that interconversion is essentially free at room temperature. Other potential energy studies[13,17] report that this barrier is between 2.0 and 5.0 kcal/mol. Also, ^{13}C-NMR relaxation experiments on ribonucleosides show that the barrier is 4.7 ± 0.5 kcal/mol for the purines.[18] Olson[13] calculated the activation energy of repuckering through an O4′-endo intermediate to be ~3.7 kcal/mol for ribose and ~2.0 kcal/mol for 2′-deoxyribose with $\nu_m = 38°$. This is consistent with X-ray data[6,8] and NMR coupling constants[10-12] which suggest that C2′-endo to C3′-endo repuckering is more difficult in ribose. This is probably due to the additional gauche effects and steric clash of the 2′-OH.

It is likely that pucker transitions occur via the pseudorotation pathway rather than through high-energy planar intermediates. A survey of furanose crystal structures of ribo- and 2′-deoxyribonucleosides and nucleoside analogues showed that ν_m is unimodally distributed, $\langle\nu_m\rangle = 38.6 \pm 3.0°$.[6] However, a fairly broad range of ν_m (30° to 46°) is observed in crystal structures.[3,6,8] Ab initio calculations on tetrahydrofuran showed that repuckering at constant ν_m gave the lowest activation energy.[19] While it is also possible to calculate reasonable activation energies for repuckering in substituted furanoses at constant ν_m,[13,15,16] this is not strictly correct, since it is known that ν_m is dependent on P.[5,7,14] For example, ν_m can be as low as 20° as the sugar passes through the high-energy O4′-exo (P = 270°) barrier.[14] At the more accessible O4′-endo (P = 90°) barrier, however, there is conflicting data. Levitt and Warshel[14] predict that ν_m decreases to approximately 35° at O4′-endo while Harvey and Prabhakaran[5] report an increase in $\langle\nu_m\rangle$ to about 50°. The latter study[5] examined ribose dynamics within a tRNA molecule, so it may not accurately reflect the behavior of free sugars.

The N-glycosidic linkage (χ) is another major degree of freedom in nucleosides. The IUPAC definition of the glycosidic torsion, χ, consists of atoms O4′–C1′–N9–C4 for purines and O4′–C1′–N1–C2 for pyrimidines. Like the furanose ring, the χ torsion also has two preferred states: anti (χ = −135° to −180°) and syn (χ = 0° to 45°). There are two barriers to interconversion between anti and syn: high anti (χ = −90°) and high syn (χ = 90°).[20] A nanosecond relaxation process detected in purine nucleosides by ultrasonic analysis is attributed to anti to syn interconversion, since this process is not present for pyrimidine nucleosides.[21,22] NMR and CD solution studies have determined that the anti to syn transition is rapid for purine nucleosides.[23-30] It is known from crystallographic analysis[6] and potential energy calculations[16,31] that it is sterically difficult, though not impossible,[25,32] for pyrimidine nucleosides to attain the syn conformation.

It is difficult to determine whether P, ν_m, and χ are energetically coupled using available steady-state solution methods. Purine nucleosides which crystallize C2′-endo adopt anti or syn conformations equally whereas the anti conformation is preferred for C3′-endo sugars.[6] Circular correlation and regression analysis of available crystal structures suggest that nearly all torsional changes in nucleosides are concerted.[33] We chose to test whether P, χ, and ν_m are coupled during the C2′-endo/anti to C3′-endo/syn transition using molecular modeling methods. Potential energy surfaces of $V(P,\chi)$ were constructed with ν_m fixed at 39° to determine possible pathways and activation energies for this transition. Also, free energy surfaces of PMF(P,χ) were generated so that transition pathways could be determined dynamically with ν_m unconstrained. Our results suggest that P and χ are not energetically coupled in the most plausible pathways from C2′-endo/anti to C3′-endo/syn. Finally, ν_m provides an entropic contribution to dN flexibility.

Methods

All calculations were performed on either a Silicon Graphics Iris 4D-440/GTX with two 40-MHz and two 20-MHz processors or a SGI Personal Iris computer. An in-house molecular mechanics program written in Fortran77 was used in all simulations and statistical calculations.

Potential Function and Force Field. We used a combination of methods to examine conformational transitions in both potential and free energy hyperspace. As with most molecular mechanics studies, the potential function and force field are central to all calculations.[34] The following standard potential function was used to calculate potential energy and forces as a function of bond lengths, bond angles, torsional rotation, and van der Waals and electrostatic interactions

$$V = \sum k_{\text{bonds}}(b - b_0)^2 + \sum k_{\text{angles}}(\alpha - \alpha_0)^2 + \sum k_{\text{dihedrals}}[1 + \cos(n\phi - \delta)] + \sum\left[\frac{A}{r^{12}} - \frac{B}{r^6} + \frac{322q_1q_2}{\epsilon r}\right] \quad (5)$$

The first two terms of eq 5 are Hooke's Law harmonic functions to maintain bonds and angles near some equilibrium value. A periodic cosine term simulates the trans minimum and eclipsed maxima for rotation about a covalent bond. The last two terms of the potential function account for most of the computation time spent in molecular mechanics calculations. A 6–12 Lennard-Jones potential simulates van der Waals repulsion–dispersion. The A and B constants are calculated from atomic radii and potential well depths for individual atom pairs. We applied a "lattice-compression" correction[35] to the A and B constants used in energy minimization as described by Schlick.[36] A_{ij} and B_{ij} constants are calculated from the sum of the van der Waals radii, r, of atoms i and j plus 0.2 Å

$$A_{ij} = V_{ij}(r_{ij} + 0.2)^{12}$$

$$B_{ij} = 2V_{ij}(r_{ij} + 0.2)^6$$

where V_{ij} is the potential energy well.

(15) Schlick, T.; Peskin, C.; Broyde, S.; Overton, M. *J. Comput. Chem.* **1987**, *8*, 1199–1224.
(16) Pearlman, D. A.; Kim, S.-H. *J. Biomol. Struct. Dyn.* **1985**, *3*, 99–125.
(17) Broyde, S.; Wartell, R. M.; Stellman, S. D.; Hingerty, B. *Biopolymers* **1978**, *17*, 1485–1506.
(18) Roder, O.; Ludemann, H.-D.; von Goldammer, E. *Eur. J. Biochem.* **1975**, *53*, 517–525.
(19) Cremer, D.; Pople, J. A. *J. Am. Chem. Soc.* **1975**, *97*, 1358–1367.
(20) Saenger, W. *Principles of Nucleic Acid Structure*; Springer-Verlag: New York, 1984. The reader is referred to Chapter 4 of this reference for a more complete description of the N-glycosidic linkage.
(21) Hemmes, P. R.; Oppenheirmer, L.; Jordan, F. *J. Am. Chem. Soc.* **1974**, *96*, 6023–6026.
(22) Rhodes, L. M.; Schimmel, P. R. *Biochemistry* **1971**, *10*, 4426–4433.
(23) Ludemann, H.-D.; Westhof, E. *Nuclear Magnetic Resonance Spectroscopy in Molecular Biology*; Pullman, B., Ed.; D. Reidel Publishing Company: Dordrecht, Holland, 1978.
(24) Ludemann, H.-D.; Westhof, E.; Roder, O. *Eur. J. Biochem.* **1974**, *49*, 143–150.
(25) Schweizer, M. P.; Banta, E. B.; Witkowski, J. T.; Robins, R. K. *J. Am. Chem. Soc.* **1973**, *95*, 3770–3778.
(26) Kondo, N. S.; Fang, K. N.; Miller, P. S.; Ts's, P. O. P. *Biochemistry* **1972**, *11*, 1991–2003.
(27) Miles, D. W.; Townsend, L. B.; Miles, D. L.; Eyring, H. *Proc. Natl. Acad. Sci. U.S.A.* **1979**, *76*, 553–556.
(28) Ezra, F. S.; Lee, C. H.; Kondo, N. S.; Danyluk, S. S.; Sarma, R. H. *Biochemistry* **1977**, *16*, 1977–1987.
(29) Hart, P. A.; Davis, J. P. *Jerusalem Symp. Quantum Chem. Biochem.* **1973**, *5*, 297–310.
(30) Ts'o, P. O. P.; Kondo, N. S.; Schweizer, M. P.; Hollis, D. P. *Biochemistry* **1969**, *8*, 997–1029.
(31) Haschemeyer, A. E. V.; Rich, A. *J. Mol. Biol.* **1967**, *27*, 369–384.
(32) Saenger, W.; Scheit, K. H. *J. Mol. Biol.* **1970**, *50*, 153–169.
(33) Kitamura, K.; Wakahara, A.; Mizuno, H.; Baba, Y.; Tomita, K. *J. Am. Chem. Soc.* **1981**, *103*, 3899–3904.
(34) McCammon, J. A.; Harvey, S. C. *Dynamics of Proteins and Nucleic Acids*; Cambridge University Press: New York, 1987.
(35) Pauling, L. *The Nature of the Chemical Bond*; Cornell University Press: New York, 1960. Olson, W. K.; Flory, P. J. *Biopolymers* **1972**, *11*, 25–56. Allinger, N. L. *Adv. Phys. Org. Chem.* **1976**, *13*, 1–85.
(36) Schlick, T. Ph.D. Thesis, New York University, 1987.

Table I. Endocyclic Torsion Parameters

		n	K_ϕ (kcal/mol)
ν_0	C4′–O4′–C1′–C2′	3	1.8
ν_1	O4′–C1′–C2′–C3′	3	2.8
		2	0.2
	O4′–C1′–C2′–O2′ [a]	2	1.0
ν_2	C1′–C2′–C3′–C4′	3	2.8
	C1′–C2′–C3′–O3′	2	0.2
	O2′–C2′–C3′–O3′ [a]	2	1.0
ν_3	C2′–C3′–C4′–O4′	3	2.8
		2	0.2
	O3′–C3′–C4′–O4′	2	1.0
	O3′–C3′–C4′–C5′	2	0.2
ν_4	C3′–C4′–O4′–C1′	3	1.8

[a] Gauche torsions necessary in ribose.

$$V_{ij} = (V_i V_j)^{1/2}$$

Standard A and B constants were used in MD calculations. Electrostatic field strength is calculated by Coulomb's Law for all atom pairs separated by three or more bonds.

Force constants, equilibrium values, and partial charges from the explicit hydrogen AMBER force field[37] were used for this study. Since we were modeling small systems (i.e. deoxynucleosides, ~35 atoms), no nonbond cutoff distance was imposed. All calculations were done in vacuo with a constant dielectric ($\epsilon = 4.0$). A distance-dependent dielectric constant was also tested, but the results were essentially identical (data not shown). 1–4 nonbond interactions (i.e. atoms separated by three bonds) were not scaled in our calculations. We scaled 1–4 interactions initially by 50% as in Weiner et al.[37] but found that 0% scaling gave results more consistent with experimental data.[38] Finally, the gauche effect described by Olson[13] was simulated by assigning additional two-fold ($n = 2$) parameters to endocyclic torsions containing a terminal oxygen (Table I). Inclusion of two-fold parameters is necessary to account for the gauche conformational preference of these torsions. It is worth noting that the above parameters were extensively tested for both 2′-deoxyribose and ribose using both energy minimization and molecular dynamics before the bases were attached.

Conformational Space Searching. A. Molecular Dynamics (MD). We used MD to sample conformational space for the dN's. This method ignores the quantum mechanical contributions of electrons, which are treated implicitly in the potential function, and treats nuclei as point charges and masses. Thus, Newton's equations of motion can be used to determine the trajectory of each atom from the net force acting on the atom with respect to time. See McCammon and Harvey[34] for a more detailed description of MD. However, the equations of motion must be approximated numerically for systems larger than two independent particles (i.e. the many-body problem). Since the net force acting on the molecule is zero, the total energy of the system must be conserved in spite of numerical round-off error. We used the Verlet algorithm[39] to integrate the equations of motion in our dynamics program. With a 1-fs time step, the total energy (potential plus kinetic) of the system was conserved in all MD simulations.

There are three stages in an MD simulation: heating, equilibration, and production or "free dynamics." Each dN molecule was heated from 5 to 300 K over 1 ps. In MD calculations, the molecule is coupled to an artificial "solvent bath" by randomly assigning velocities to each atom corresponding to a Maxwellian distribution about a mean target temperature. For our simulations, random assignment of velocities was performed every 50 steps with the target temperature slowly increasing. After heating, the molecules were equilibrated for 2 ps until the temperature approached 300 ± 25 K. During equilibration, velocities were scaled rather than randomly reassigned. Every 50 steps the temperature of the molecule was checked. If the temperature was less than 275 K or greater than 325 K, all velocities were scaled up or down. Otherwise, the trajectory was allowed to continue without interference. Velocities are not reassigned or scaled during the production phase. If the equilibration was successful and the program conserves energy, velocities may fluctuate freely in the production phase and the average temperature should be near the desired value. We find the above protocol sufficient for dN's.

Data were collected during the free dynamics phase of the MD simulations. A total of twenty 1-ns simulations were performed for each dN in order to sample thermodynamically accessible regions of conformational space. We chose to use 20 × 1 ns simulations rather than a single 20-ns simulation because better sampling of phase and χ was obtained. Also, identical rates (ns^{-1}) of repuckering and anti to syn interconversion occur for the 20-ns simulation as in the 20 × 1 ns simulations. So, we concluded that both parameters had converged after 1 ns. At each step of dynamics, P and ν_m were calculated by the Rao et al.[4] method along with χ. For each 1-ns simulation all 10^6 data points were plotted for χ vs P. These plots were partitioned into 36 × 36 grids, and the potential of mean force[40] of each 10° × 10° section was calculated by the following equation

$$\Delta G = -RT \ln\left(\frac{P_{ij}}{P_H}\right) \tag{6}$$

where P_{ij} is the population of section i,j, P_H is the population of highest sampling, R is the gas constant, and T is the average temperature of the simulation. The free energy data from all twenty 1-ns simulations were averaged, and the Mathematica package (Wolfram Research, Inc., Champaign, IL) was used to generate PMF(P,χ) contour surfaces. In addition, $\langle\nu_m(P)\rangle$ was determined from all simulations.

B. Adiabatic Mapping. We used adiabatic mapping[34] to generate potential energy surfaces, $V(P,\chi)$. This method simply uses energy minimization to determine the energy change as specific parameters are altered incrementally. In this case, each dN was minimized to a starting conformation of $P = 0°$ and $\chi = -180°$. Next, both parameters were altered 360° in 10-deg increments with energy minimization after each move, thus generating a 37 × 37 grid of potential energies for the full range of P (0° to 360°) and χ (−180° to 180°).

In order to constrain individual torsions at specific values, an additional harmonic term was included in the potential energy function (eq 5). To avoid singularities at torsion angles of 0° and ±180°, we used the Taylor expansion formulation described in Brooks et al.[41] P was transformed into torsional constraints using the following equations

$$\nu_0 = \nu_m \cos(P + 72°) \tag{7}$$

$$\nu_1 = -\nu_m \cos(P + 36°) \tag{8}$$

$$\nu_2 = \nu_m \cos(P) \tag{9}$$

$$\nu_3 = -\nu_m \cos(P - 36°) \tag{10}$$

$$\nu_4 = \nu_m \cos(P - 72°) \tag{11}$$

It can be seen in these equations that it is necessary to chose ν_m in advance. So, adiabatic maps were built for each dN with $\nu_m = 39°$. Finally, we used two first-derivative iterative descent methods in our EM protocol: steepest descent and conjugate gradient.[34] Each conformation was first minimized with steepest descent to relieve the worst stresses and then to convergence ($V' \leq 0.1$ kcal/mol·Å) with conjugate gradient.

Conformational Transitions. A. Ulitsky and Elber (1990) Algorithm.[42] This algorithm is a first-derivative descent method for refining a trial transition pathway represented by a string of intermediate structures on an energy surface. The gradient acting on a point k in this trial pathway is given by the following vector equation

$$\nabla V = \mathbf{i}\frac{\partial V}{\partial P} + \mathbf{j}\frac{\partial V}{\partial \chi} \tag{12}$$

where i and j are unit vectors in the P and χ directions, respectively. We now introduce a boldface notation to represent vectors. If a unit vector $\mathbf{s}^k$ is defined as $\mathbf{R}/\|R\|$ where $\mathbf{R} = \mathbf{r}_{k-1} - \mathbf{r}_{k+1}$, then, for a correct pathway, $\nabla\mathbf{V}$ is parallel to $\mathbf{s}^k$ at point k as the distance between points $k-1$ and $k+1$ approaches zero. The dot product of $\nabla\mathbf{V}$ and $\mathbf{s}^k$ is the magnitude of the gradient at point k

$$\nabla\mathbf{V}\cdot\mathbf{s}^k = \|\nabla V\| \tag{13}$$

A different form of this equation is obtained by multiplying $\|\nabla V\|$ times

(37) Weiner, S. J.; Kollman, P. A.; Nguyen, D. T.; Case, D. A. *J. Comput. Chem.* **1986**, *7*, 230–252.
(38) Olson, W. K.; Sussman, J. L. *J. Am. Chem. Soc.* **1982**, *104*, 270–278.
(39) Verlet, L. *Phys. Rev.* **1967**, *159*, 98–103.
(40) Beveridge, D. L.; Di Capua, F. M. *Annu. Rev. Biophys. Biophys. Chem.* **1989**, *18*, 431–492.
(41) Brooks, B. R.; Bruccoleri, R. E.; Olafson, B. D.; States, D. J.; Swaminathan, S.; Karplus, M. *J. Comput. Chem.* **1983**, *4*, 187–217.
(42) Ulitsky, A.; Elber, R. *J. Chem. Phys.* **1990**, *92*, 1510–1511.

the unit vector $\mathbf{s}^k$ to give $\nabla\mathbf{V}$

$$\|\nabla V\|\mathbf{s}^k = \nabla\mathbf{V} \tag{14}$$

Substituting eq 13 into eq 14 and subtracting $(\nabla\mathbf{V}\cdot\mathbf{s}^k)\mathbf{s}^k$ from both sides gives the Ulitsky and Elber equation

$$(\nabla\mathbf{V}\cdot\mathbf{s}^k)\mathbf{s}^k = \nabla\mathbf{V}$$

$$(\nabla\mathbf{V}\cdot\mathbf{s}^k)\mathbf{s}^k - (\nabla\mathbf{V}\cdot\mathbf{s}^k)\mathbf{s}^k = \nabla\mathbf{V} - (\nabla\mathbf{V}\cdot\mathbf{s}^k)\mathbf{s}^k$$

$$0 = \nabla\mathbf{V} - (\nabla\mathbf{V}\cdot\mathbf{s}^k)\mathbf{s}^k = \nabla\mathbf{V}_{\text{projected}} \tag{15}$$

Thus, if the trial pathway is incorrect (i.e. $\nabla\mathbf{V}_{\text{projected}} \neq 0$ at point k), point k is moved to satify eq 15. Specifically, point k is moved in the direction of the vector $-\nabla\mathbf{V}_{\text{projected}}$ on the potential energy surface to give new values of P and χ.

As long as the gradients of the i and j components of eq 12 are known, $\nabla\mathbf{V}$ can be calculated and hence $\nabla\mathbf{V}_{\text{projected}}$. A simple numerical approximation was used for the i and j components of $\nabla\mathbf{V}$

$$\frac{\partial V}{\partial P} = \frac{dV}{dP}\bigg|_\chi \approx \frac{V_2 - V_1}{\Delta P}\bigg|_\chi \tag{16}$$

$$\frac{\partial V}{\partial \chi} = \frac{dV}{d\chi}\bigg|_P \approx \frac{V_2 - V_1}{\Delta \chi}\bigg|_P \tag{17}$$

where V_1 and V_2 are determined by changing P or χ slightly while keeping the other constant. So, eq 15 is solved iteratively until $\nabla\mathbf{V}_{\text{projected}}$ approaches zero within a specified tolerance for each point on the pathway. Several ten-point trial pathways were minimized on the $V(P,\chi)$ surfaces of each dN to determine the activation energies of the different C2′-endo/anti to C3′-endo/syn transition pathways.

B. CONTRA MD Algorithm.[43] Whereas the Ulitsky and Elber[42] algorithm searches for the minimum-energy pathway between two conformations on a potential energy surface, it suffers from the same problem inherent to all first-derivative methods. Namely, the optimization stops at the first minimum encountered and this minimum is influenced by the starting coordinates, in this case the initial trial pathway. While this method does give useful information about activation energies, it does not give information about relative pathway preferences in the presence of thermal motion. Also, it is necessary to constrain ν_m when calculating dV/dP in eq 16. We used the CONTRA MD (CONformational TRAnsitions using MD with minimum biasing) algorithm[43] to seek out possible transition pathways on the PMF(P,χ) surfaces of the dN's.

The CONTRA MD algorithm is conceptually very simple. To begin, all that is required is an initial conformation and a function that measures progress along the pathway of the transition being studied. Starting from the initial conformation, a short free MD run is carried out to produce a trial trajectory. If the system moves toward the desired conformation, the trajectory is saved, the atomic positions at the end of this trial run define the starting conformation for the next increment of the MD simulation, and the trajectory is continued. If the trial trajectory moves away from the desired conformation, this piece of the trajectory is deleted, the atomic positions are reset to those of the initial conformation, and the atomic velocities are reassigned. This procedure is repeated over and over, producing a series of structures that evolve toward the target conformation. To model a transition from an initial to a final conformation requires the definition of a function that measures position along the transition pathway. We designate the measuring function by M, which is calculated from P and χ

$$M = [(P - P_T)^2 + (\chi - \chi_T)^2]^{1/2}$$

where P_T and χ_T are the desired final values. There are two requirements on the measuring function. First, given any set of atomic positions, the function must be single valued. Second, it must be known whether the conformational change leads to an increase or a decrease in M.

We ran 100 CONTRA MD simulations at 300 K using the same heating and equilibration protocol described above and a 50-step trial trajectory for each dN to determine the relative pathway preferences for a C2′-endo/anti to C3′-endo/syn transition.

Results and Discussion

Ribose and 2′-Deoxyribose. A. Adiabatic Mapping. Consistent with experimental data,[38] adiabatic maps of $V(P)$ for $\nu_m = 39°$

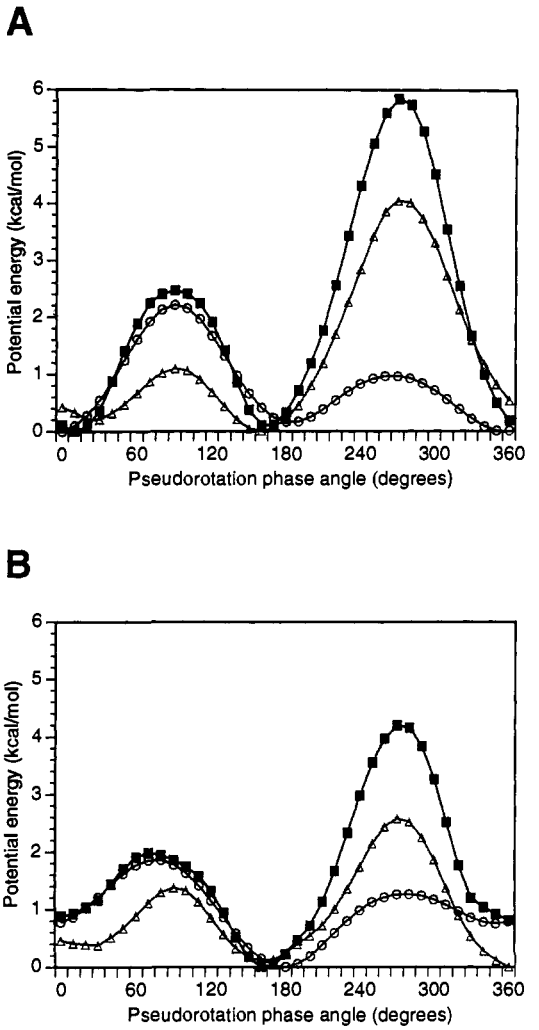

Figure 1. Adiabatic maps $V(P)$ for ribose (A) and 2′-deoxyribose (B). ν_m is fixed at 39°. The plots show total energy from eq 5 (■), three-fold plus two-fold torsional energy (○), and nonbond energy (△). Both sugars have minima at C3′-endo (P = 0–30°) and C2′-endo (P = 150–180°). Notice that torsional energy dominates at the O4′-endo barrier (P = 90°) and nonbond energy dominates at the O4′-exo barrier (P = 270°).

show minima at C2′- and C3′-endo for ribose and 2′-deoxyribose (Figure 1). Ribose has a slight preference for C3′-endo (Figure 1A) while the more asymmetric 2′-deoxyribose shows a pronounced preference for C2′-endo (Figure 1B). The energy barrier for interconversion is higher for ribose compared to 2′-deoxyribose. This is due to steric clash between the two hydroxyl groups and is responsible for the decreased flexibility of ribose as suggested by Olson.[13] Our results, however, show that torsional stress is the dominant energy term for interconversion through the O4′-endo intermediate while nonbond energy dominates at the O4′-exo barrier (Figure 1). Recall from Table I that additional two-fold gauche torsions are necessary for ribose because of the 2′-OH group. This result is similar to those of Nilsson and Karplus[44] using the EF2 force field and Schlick using a nonstandard potential function.[15,36]

To examine the energetic dependence of P on ν_m, we built adiabatic maps at several values of ν_m. Recall from eqs 7–11 that it is necessary to choose ν_m in order to constrain the furanose at a particular value of P. Figure 2 shows adiabatic maps of ribose (Figure 2A) and 2′-deoxyribose (Figure 2B) at various values of ν_m. It can be seen that ν_m has little effect on the O4′-endo barrier in the range of ν_m = 37°–45° for both sugars. As ν_m decreases

(43) Harvey, S. C.; Gabb, H. A. *Biopolymers*, in press.

(44) Nilsson, L.; Karplus, M. *J. Comput. Chem.* **1986**, *7*, 591–616.
(45) Young, D. W.; Tollin, P.; Wilson, H. R. *Nature* **1974**, *248*, 513–514. Viswamitra, M. A.; Seshadri, T. P. *Nature* **1974**, *252*, 176–177.

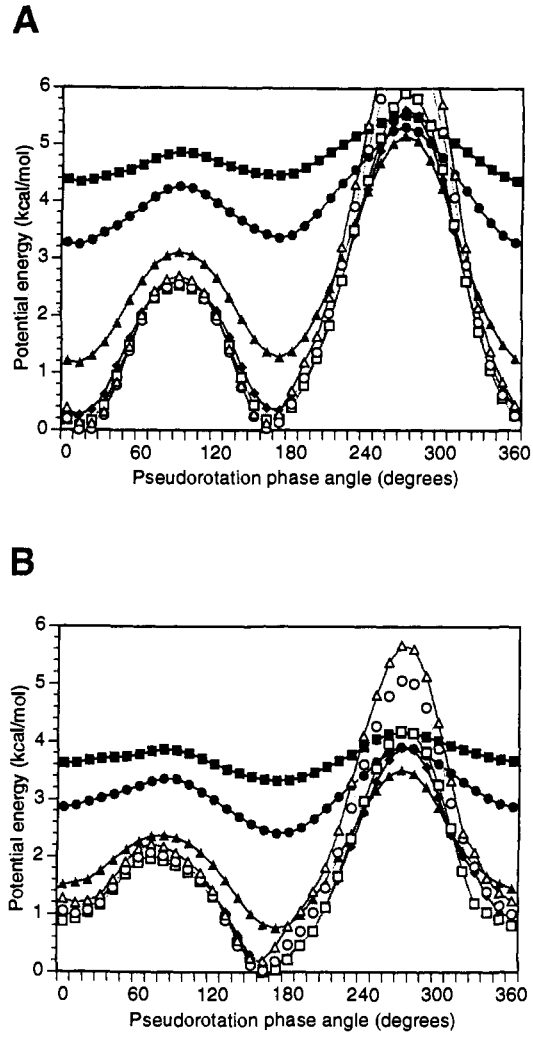

Figure 2. Adiabatic maps $V(P)$ for ribose (A) and 2′-deoxyribose (B) at various ν_m. Each curve shows the potential energy for a given value of ν_m: 15° (■), 21° (●), 31° (▲), 37° (◆), 39° (□), 43° (○), and 45° (△). In general, higher ν_m is advantageous for transitions via O4′-endo intermediates while lower ν_m is better at O4′-exo.

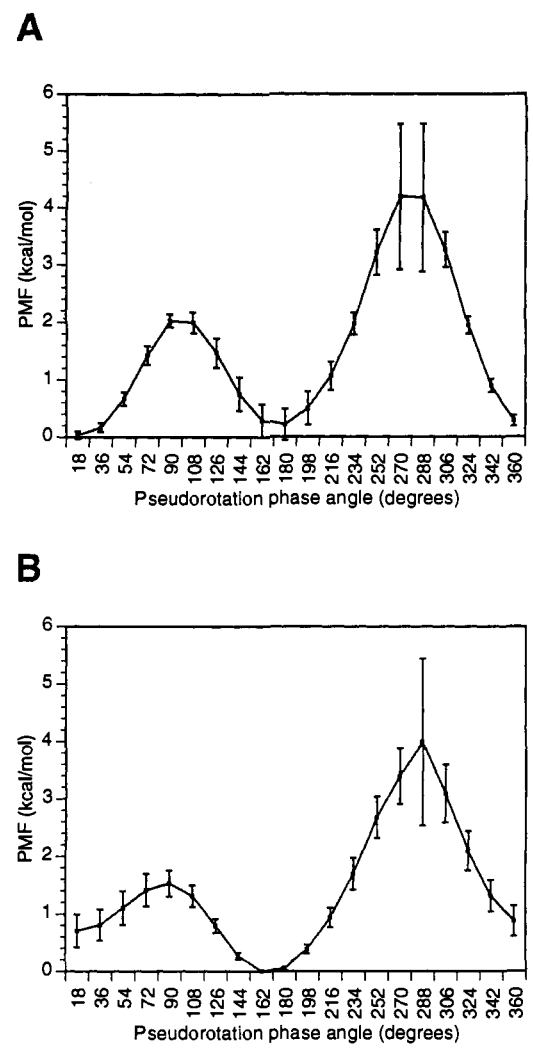

Figure 3. Dynamics data PMF(P) for ribose (A) and 2′-deoxyribose (B). The standard deviations of the mean PMF in each 18-deg section from 20 1-ns MD simulations is shown.

below 37°, however, energies increase throughout most of pseudorotation phase space except near the O4′-exo barrier. In this area, high ν_m leads to increases in nonbond energy, the dominant energy at P = 270° (Figure 1), and artificially high barriers at O4′-exo. This is not too important for ribose where the P = 90° and P = 270° barriers are considerably different (~2.6 kcal/mol). It is significant for 2′-deoxyribose, however, where these barriers are only 1.4 kcal/mol apart. Also, notice that ν_m has a slight effect on the location of the minima for both sugars. It is difficult to model furanose rings accurately using only minimization methods, since fixing P requires that ν_m also be fixed.

B. Molecular Dynamics. The measure of a force field is its performance during MD calculations, since free energy hyperspace reflects the true behavior of the molecule, not potential energy space.[46] Specifically, are experimental parameters still satisfied when kinetic energy is added to the system? There are two advantages to using MD to model sugars and nucleosides. First, these systems are sufficiently small that long simulations (i.e. nanosecond timescale) are possible. Thus, much more of conformational space is sampled and thermodynamic ensembles can be generated. Second, ν_m may fluctuate during MD calculations. So, ν_m preferences as a function of P can be determined dynamically. The Helmholtz free energy, or more appropriately the potential of mean force,[40] as a function of P was calculated from the Boltzmann distributions of 20 1-ns simulations (Figure 3). A comparison of Figures 1 and 3 shows that the PMF(P) and $V(P)$ profiles are similar in shape but not in magnitude. Barrier heights are reduced in the presence of thermal motion. This would imply that entropy is important for interconversion between C2′-endo and C3′-endo. Also, since ν_m is free to adapt to changes in P, the O4′-endo and especially the O4′-exo regions are more accessible. Preferred ν_m ranges for ribose and 2′-deoxyribose are shown in Figure 4. $\langle\nu_m\rangle$ is nearly constant for repuckering of 2′-deoxyribose via an O4′-endo (P = 90°) intermediate but fluctuates ~±2° for ribose. $\langle\nu_m\rangle$ decreases drastically for both sugars near the O4′-exo (P = 270°) barrier.

Both sugars repucker freely during MD calculations at 300 K. Ribose and 2′-deoxyribose interconvert between C2′- and C3′-endo at rates of 28 ± 8 and 142 ± 38 ns^{-1}, respectively. However, since explicit water molecules were not included in our simulations, these rates are probably artificially high. We chose to use implicit rather than explicit solvent models because the latter are too computationally demanding to generate thermodynamic ensembles even for small systems.

2′-Deoxynucleosides. Satisfied that our force field is properly parametrized for furanose rings, the bases were added to 2′-deoxyribose so that we could answer our original question: Are the C2′-endo to C3′-endo and anti to syn transitions energetically coupled in 2′-deoxynucleosides?

(46) Tran-Dinh, S.; Guschlbauer, W.; Gueron, M. *J. Am. Chem. Soc.* **1972**, *94*, 7903–7911.

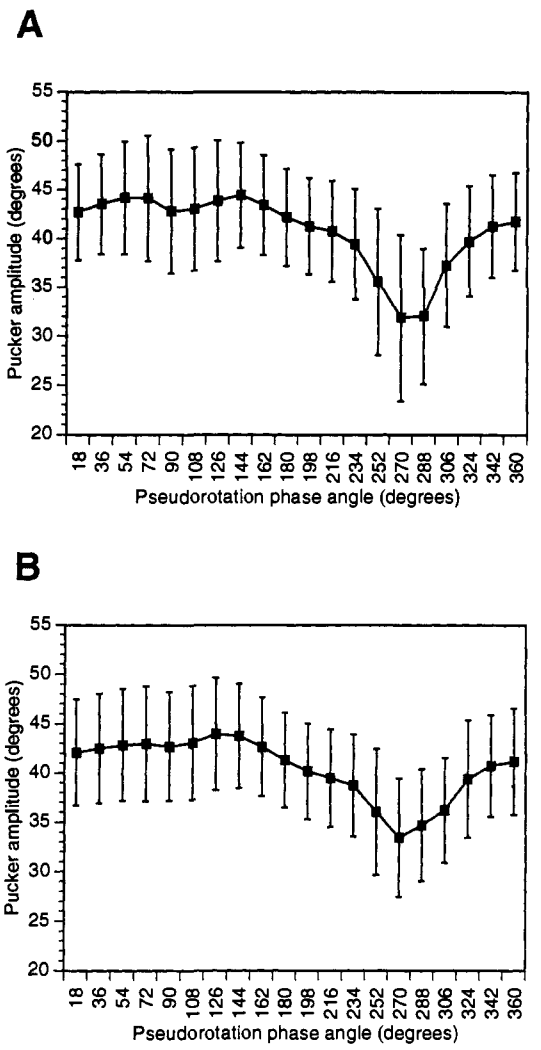

Figure 4. Average $\nu_m(P)$ for ribose (A) and 2′-deoxyribose (B). The standard deviation in ν_m for all 20 1-ns MD simulations is shown for each 18-deg section. Notice that ribose requires slightly larger changes in ν_m throughout P space. Both sugars require large reductions in ν_m to cross the O4′-exo barrier.

A. 2′-Deoxyadenosine (dA). The $V(P,\chi)$ adiabatic map for dA at $\nu_m = 39°$ is shown in Figure 5A. The global minimum is in the C2′-endo/anti (I) region of the potential energy surface. Other minima are, in order of ascending energy, C2′-endo/syn (II), C3′-endo/anti (III), and C3′-endo/syn (IV). This is similar to the result of Pearlman and Kim,[16] who used a different force field and molecular representation, except that we found no minima at C2′-endo/$\chi \sim -45°$ or C3′-endo/$\chi \sim -45°$. Four possible transition pathways from C2′-endo/anti to C3′-endo/syn are evident from the contour map (Figure 5B). We used the Ulitsky and Elber[42] refinement algorithm to minimize approximate pathways and determine the corresponding energy fluctuations of each path (Figure 5C). Obviously, paths 1 and 2 require less energy than paths 3 and 4 and are the most probable. Also, the C2′-endo/anti to C3′-endo/syn transition most likely occurs through O4′-endo and high anti intermediates. It is important to note at this point that repuckering and the anti to syn transition occur nearly independently for paths 1, 2, and 3 (Figure 5B). In path 2 there is a slight dependence of χ on P near $\chi \sim -45°$. In path 4, however, χ must assume a narrow range of values before repuckering can occur.

We ran 20 1-ns MD simulations at 300 K for dA to determine PMF(P,χ) in the presence of thermal motion and the entropy associated with unconstrained ν_m. PMF(P,χ) (Figure 5D) and $V(P,\chi)$ (Figure 5A) are qualitatively similar. From adiabatic mapping, repuckering and the anti to syn N-glycosidic transition appear to be nearly independent events for the two most probable pathways (Figure 5B,C). The rates of repuckering and the N-glycosidic transition from the MD simulations are 94 ± 16 and 35 ± 9 ns^{-1}, respectively. This might suggest that repuckering occurs first, since it is more rapid and energetically cheaper. To test this hypothesis, we used the CONTRA MD algorithm[43] to induce the C2′-endo/anti to C3′-endo/syn transition and measure the propensity for the available pathways. After 100 transitions, path 1 was preferred over paths 2, 3, and 4 by a ratio of 51:47:2:0. There is really no significant difference between paths 1 and 2. Finally, since the rate of repuckering for dA is within one standard deviation of that of 2′-deoxyribose, furanose flexibility is not drastically affected by the presence of a base. Also, $\nu_m(P)$ for dA (Figure 5E) is very similar to $\nu_m(P)$ for 2′-deoxyribose (Figure 4B).

B. 2′-Deoxyguanosine (dG). It is readily apparent from Figure 6 that the conformational flexibility of dG is similar to that of dA. However, the global minimum is C2′-endo/syn, and additional minima are present in the $V(P,\chi)$ adiabatic map of dG (Figure 6A) at C3′-endo/$\chi \sim -45°$ (VI) and C2′-endo/$\chi \sim -45°$ (V). The source of difference in global minima for dA and dG is an electrostatic interaction between the O5′ and the N2 amino hydrogens in guanine. This has already been observed experimentally. 2′-Deoxyguanosine monophosphate, for example, crystallizes in the syn configuration.[45] Guanylic acid in solution also prefers the syn configuration.[46] Previous potential energy calculations show this same result for both the guanine nucleotide[47] and 2′-deoxynucleoside.[16] The preference for anti or syn at C2′-endo is negligible for both purines. For example, the C2′-endo/syn global minimum for dG is only 0.18 kcal/mol lower than the minimum at C2′-endo/anti. Also, the high syn barrier is slightly greater for dG. Four possible transition pathways from C2′-endo/anti to C3′-endo/syn are evident from the $V(P,\chi)$ surface (Figure 6B). Trial pathways were refined using the Ulitsky and Elber (1990) algorithm and the corresponding activation energies plotted (Figure 6C). Paths 1 and 2 have similar energy costs and are the most obvious means of C2′-endo/anti to C3′-endo/syn transition. Repuckering and the χ transition are independent events in path 1. In path 2, however, the χ transition is slightly dependent on P around $\chi = -45°$, similar to dA.

A PMF(P,χ) energy surface was generated for dG from 20 1-ns MD simulations at 300 K (Figure 6D). The minima are in the same places as in the $V(P,\chi)$ surface; but the global minimum has shifted to C2′-endo/anti, and the minima at C2′-endo/$\chi \sim -45°$ and C3′-endo/$\chi \sim -45°$ have disappeared. The rates of repuckering and the N-glycosidic transition for dG are 109 ± 17 and 41 ± 13 ns^{-1}, respectively. These rates are similar to those of dA. To determine which event occurs first, repuckering or the anti to syn transition, we ran 100 CONTRA MD simulations on dG. Specifically, is path 1 preferred (i.e. the anti to syn transition occurs first) or is path 2 preferred (i.e. repuckering occurs first)? The ratio of paths 1, 2, 3, and 4 is 33:67:0:0. So, unlike dA, where there is no significant difference between the two pathways, dG shows a two-fold preference for the pathway in which repuckering occurs first. Finally, $\nu_m(P)$ for dG (Figure 6E) is very similar to that of dA (Figure 5E) and 2′-deoxyribose (Figure 4B), once again suggesting that the presence of base has little effect on furanose flexibility.

C. 2′-Deoxycytidine (dC). It is with the pyrimidines that the shortcomings of assumptions based on potential energy space become apparent. The $V(P,\chi)$ adiabatic map of dC (Figure 7A) has five energy minima. They are, in ascending order, C2′-endo/anti (I), C3′-endo/anti (II), C2′-endo/syn (III), C3′-endo/syn (IV), and C2′-endo/$\chi \sim -45°$ (V). Notice, however, that the C2′-endo/syn minimum is only 0.5 kcal/mol greater than the global minimum at C2′-endo/anti and is nearly equal to the

(47) Yathindra, N.; Sundaralingam, M. *Biopolymers* **1973**, *12*, 2075–2082.

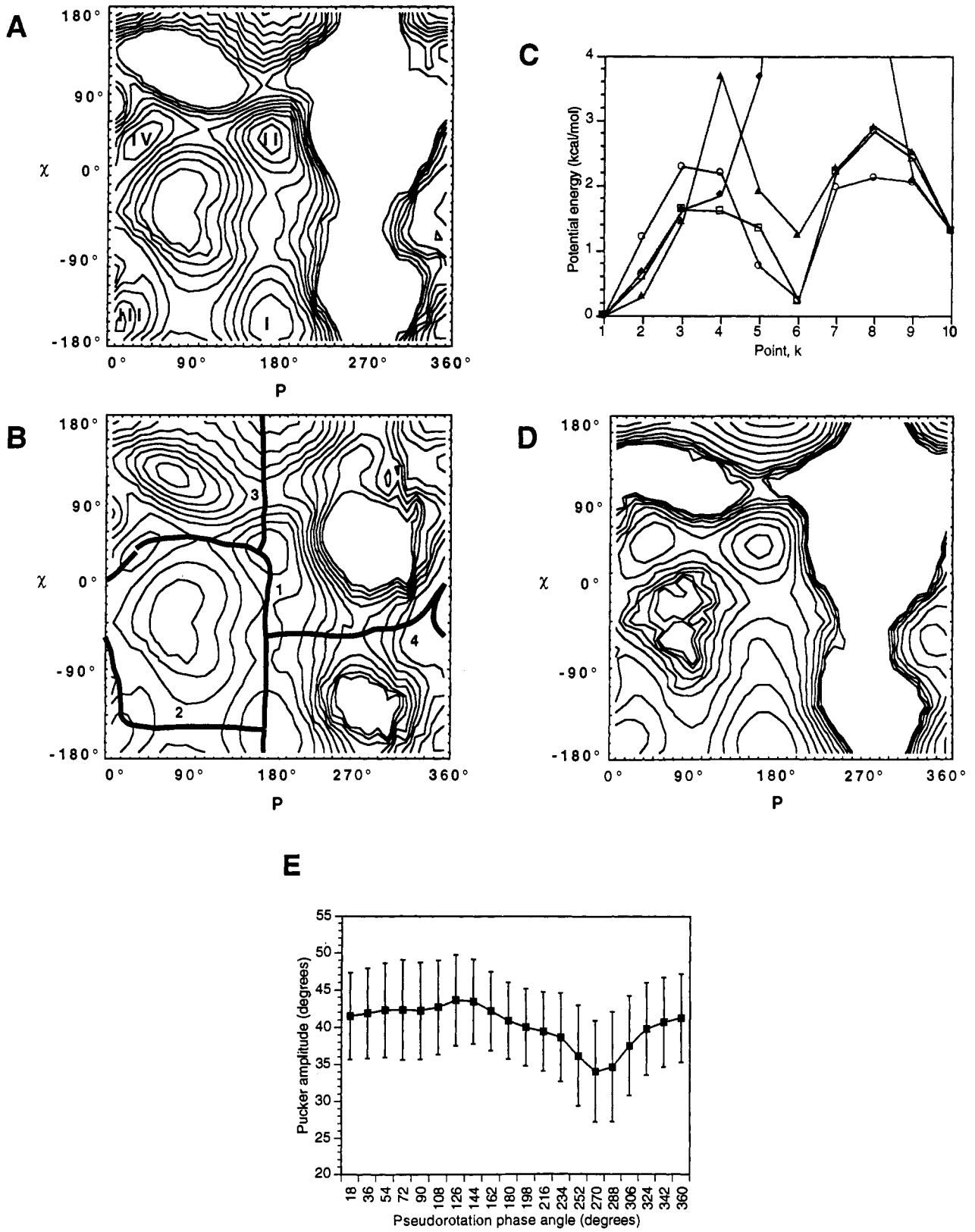

Figure 5. 2′-Deoxyadenosine. (A) Adiabatic map $V(P,\chi)$ with $\nu_m = 39°$. Potential energy is shown from 0 to 5 kcal/mol with contours at intervals of 0.5 kcal/mol. (B) $V(P,\chi)$ with $\nu_m = 39°$ showing possible transition pathways from C2′-endo/anti to C3′-endo/syn. Potential energy is shown from 0 to 10 kcal/mol with contours at intervals of 1.0 kcal/mol. (C) Potential energy fluctuations from C2′-endo/anti (point 1) to C3′-endo/syn (point 10) for the four pathways shown in B: path 1 (□), path 2 (○), path 3 (▲), and path 4 (◆). (D) Average free energy surfaces PMF(P,χ) from 20 1-ns MD simulations at 300 K. Energy is shown from 0 to 5 kcal/mol with contours at intervals of 0.5 kcal/mol. (E) Average $\nu_m(P)$ from all 20 1-ns MD simulations at 300 K.

minimum at C3′-endo/anti. While it is possible for pyrimidines to adopt the syn configuration,[25,32] it is sterically difficult[16,31] and rarely observed in nature.[6] On the basis of Figure 7A, one might conclude incorrectly that anti and syn are nearly equivalent energetic states separated by a high activation energy barrier.

A MD simulation using the same force field gives a more

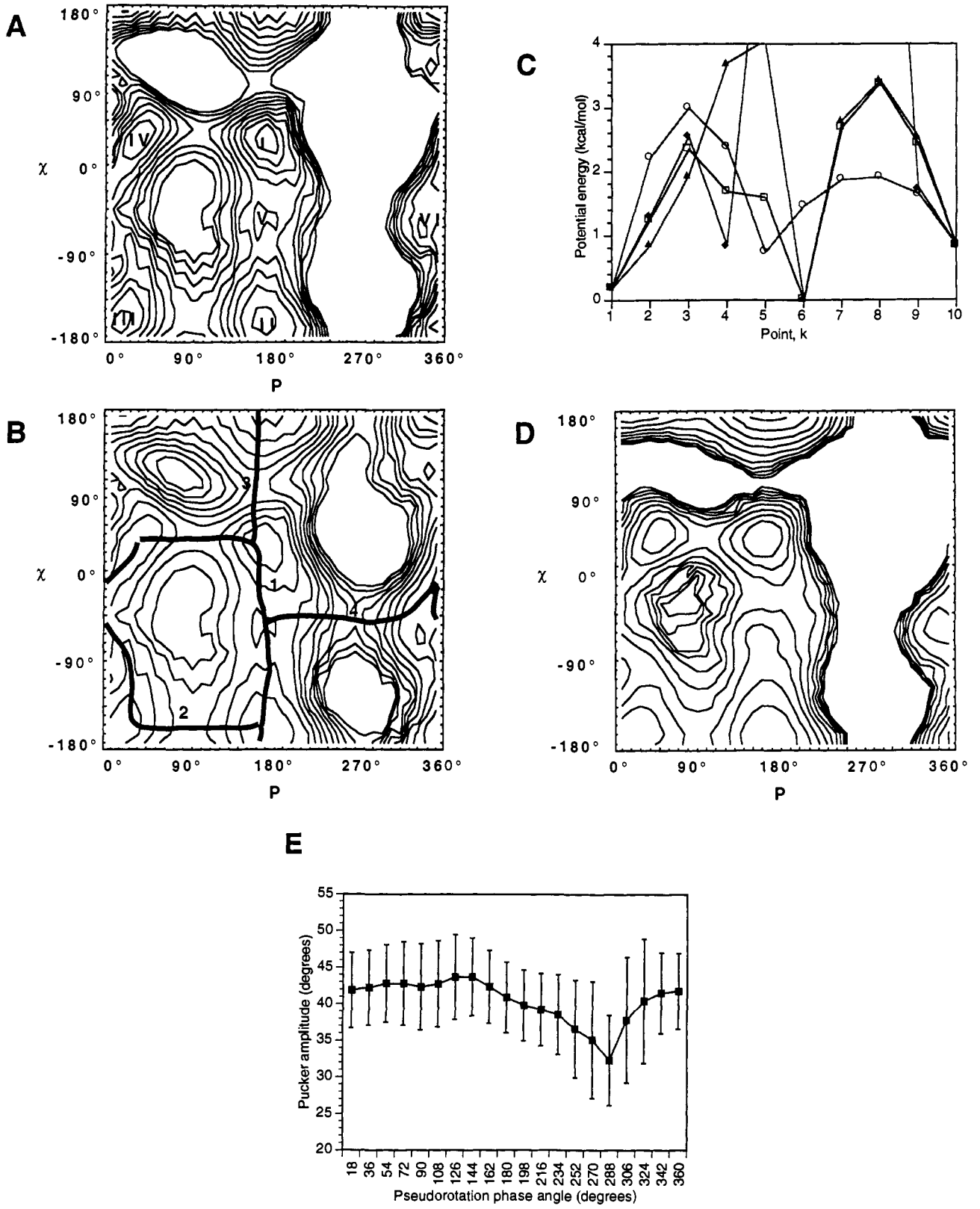

Figure 6. 2′-Deoxyguanosine. (A) Adiabatic map $V(P,\chi)$ with $\nu_m = 39°$. Potential energy is shown from 0 to 5 kcal/mol with contours at intervals of 0.5 kcal/mol. (B) $V(P,\chi)$ with $\nu_m = 39°$ showing possible transition pathways from C2′-endo/anti to C3′-endo/syn. Potential energy is shown from 0 to 5 kcal/mol with contours at intervals of 0.5 kcal/mol. (C) Potential energy fluctuations from C2′-endo/anti (point 1) to C3′-endo/syn (point 10) for the three pathways shown in B: path 1 (□), path 2 (○), path 3 (▲), and path 4 (◆). (D) Average free energy surfaces PMF(P,χ) from 20 1-ns MD simulations at 300 K. Energy is shown from 0 to 5 kcal/mol with contours at intervals of 0.5 kcal/mol. (E) Average $\nu_m(P)$ from all 20 1-ns MD simulations at 300 K.

realistic view of pyrimidine conformational accessibility. Figure 7B was constructed from 20 1-ns MD simulations at 300 K. The PMF(P,χ) surface shows about a 3.5 kcal/mol difference between anti and syn minima. Also, the minimum at C2′-endo/$\chi \sim -45°$ has disappeared. It is apparent from the PMF(P,χ) surface of dC (Figure 7B) that anti is much preferred over syn. If the two states were energetically similar, as in the $V(P,\chi)$ surface (Figure 7A), sampling in the syn regions would have been greater during

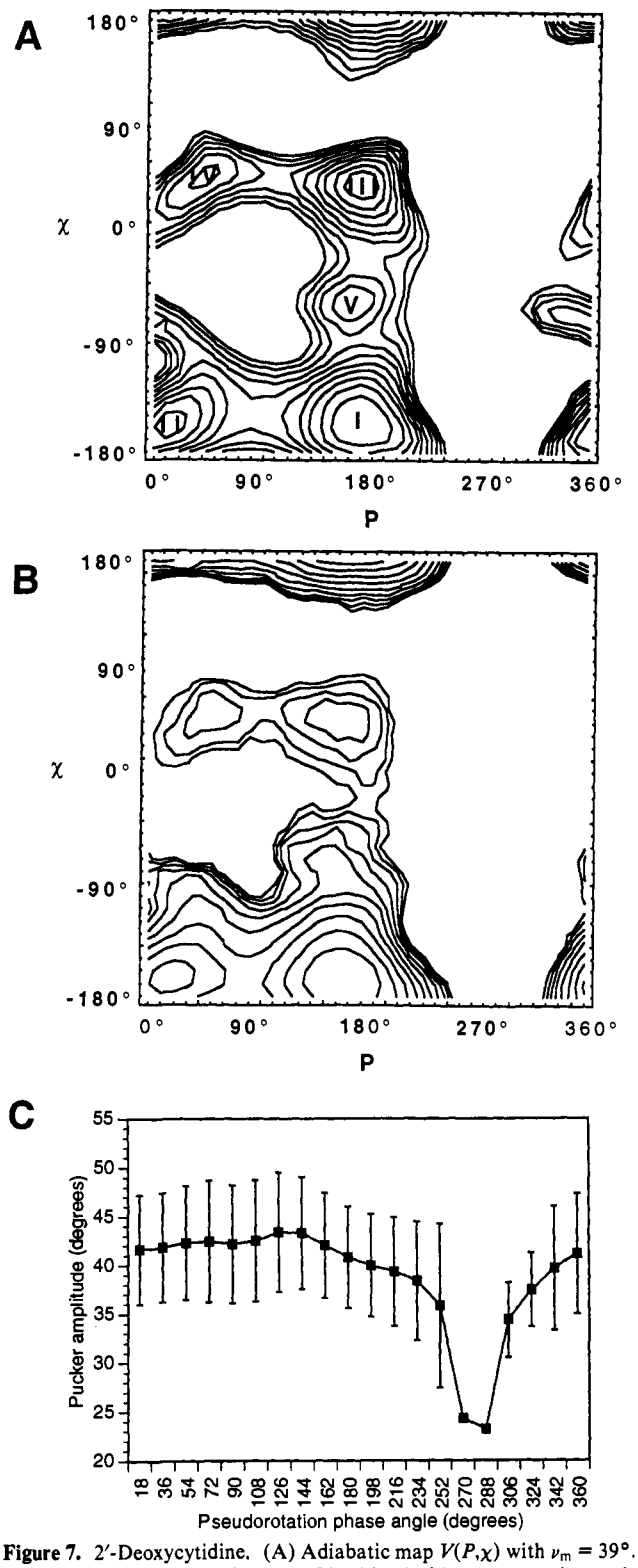

Figure 7. 2′-Deoxycytidine. (A) Adiabatic map $V(P,\chi)$ with $\nu_m = 39°$. Potential energy is shown from 0 to 5 kcal/mol with contours at intervals of 0.5 kcal/mol. (B) Average free energy surfaces PMF(P,χ) from 20 1-ns MD simulations at 300 K. Energy is shown from 0 to 5 kcal/mol with contours at intervals of 0.5 kcal/mol. (C) Average $\nu_m(P)$ from all 20 1-ns MD simulations at 300 K.

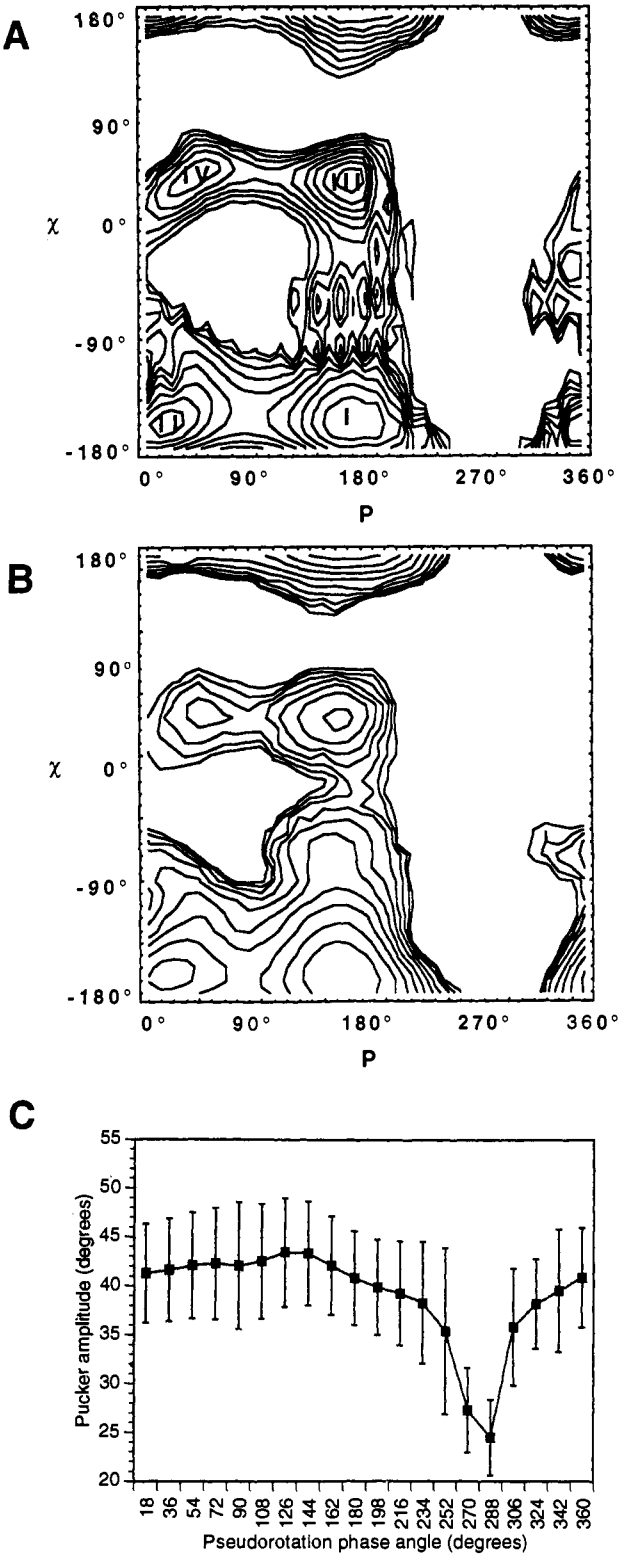

Figure 8. 2′-Deoxythymidine. (A) Adiabatic map $V(P,\chi)$ with $\nu_m = 39°$. Potential energy is shown from 0 to 5 kcal/mol with contours at intervals of 0.5 kcal/mol. (B) Average free energy surfaces PMF(P,χ) from 20 1-ns MD simulations at 300 K. Energy is shown from 0 to 5 kcal/mol with contours at intervals of 0.5 kcal/mol. (C) Average $\nu_m(P)$ from all 20 1-ns MD simulations at 300 K.

MD calculations. Recall, for example, that the potential energy barrier between C2′- and C3′-endo is approximately 2.5 kcal/mol for ribose (Figure 1A). However, there is nearly equal sampling of the two states during MD calculations. (Figure 3A), since C2′- and C3′-endo are energetically similar.

The $V(P,\chi)$ and PMF(P,χ) surfaces (Figures 7A,B) show that only one pathway is energetically feasible for a C2′-endo/anti to C3′-endo/syn transition and even this pathway is not likely to occur in nature. It is also apparent that repuckering and the N-glycosidic transition are independent events with the anti to syn transition preceeding C2′- to C3′-endo repuckering. Another indicator that repuckering and the N-glycosidic transition are unrelated is that the rate of repuckering is 123 ± 26 ns^{-1} while

that of the anti to syn transition is 3 ± 2 ns^{-1}. Since the rate of repuckering for dC is similar to the rates for purines, it is clear that the type of base has little effect on furanose flexibility in thermodynamically accessible regions of PMF(P,χ) space. In the O4′-exo region of P space, however, the larger C2–N1–C6 angle in the pyrimidine base (compared to the C4–N9–C8 angle in purines) forces drastic reductions in ν_m (Figure 7C) compared to that of 2′-deoxyribose (Figure 4A) and the purine nucleosides (Figures 5E and 6E).

D. 2′-Deoxythymidine (dT). Results obtained for dT are very similar to those for dC except that scattered and erratic minima are observed in the C2′-endo/high anti region of the $V(P,\chi)$ map (Figure 8A). Since an all-hydrogen model was used for each dN, these multiple minima are presumably due to interaction of the C5-methyl hydrogens of thymine with the C5′ substituents of the sugar. This effect is less apparent in the PMF(P,χ) surface (Figure 8B). It is apparent, however, that dT, like dC, has difficulty overcoming the barrier at C2′-endo/$\chi \sim 0°$ and reaching C2′-endo/syn during MD calculations (Figure 8B). Two possible paths exist for the C2′-endo/anti to C3′-endo/syn transition in the $V(P,\chi)$ surface (Figure 8A), but only one is available on the PMF(P,χ) surface (Figure 8B). This is expected, since it is well known that steric clash between C5′ and O2 in pyrimidines makes the syn configuration unlikely.[31] Also, the rate of repuckering, 130 ± 20 ns^{-1}, is similar to those of 2′-deoxyribose, dA, dG, and dC, indicating that furanose flexibility is not related to the presence or type of base. The rate of the anti to syn transition, 4.7 ± 2.9 ns^{-1}, shows that this transition is rare in pyrimidines. Finally, as with dA, dG, and dC, $\nu_m(P)$ for dT (Figure 8C) is similar to 2′-deoxyribose in the energetically accessible regions of PMF(P,χ) space but is drastically reduced near O4′-exo.

Conclusions

A thorough molecular modeling study was carried out to determine whether P, χ, and ν_m are energetically coupled in dN's. The AMBER explicit hydrogen force field[37] was selected and its performance extensively tested for ribose and 2′-deoxyribose using adiabatic mapping and MD calculations. This force field was chosen because it contains parameters and partial charges for all-hydrogen dN models. Also, it satisfied all available experimental data[38] for ribose and 2′-deoxyribose with only minor adjustments. Specifically, inclusion of the two-fold gauche torsions of Olson[13] was necessary for proper results (Table I, Figures 1 and 3). Testing the force field against the free sugars was essentially a positive control before addition of the bases to 2′-deoxyribose.

Molecular mechanics calculations on the four commonly occurring dN's revealed several interesting results. For example, interconversions between the C2′- and C3′-endo and anti and syn configurations are essentially independent events in the pyrimidine nucleosides (Figures 7 and 8) and are predominantly so in the purine nucleosides (Figures 5 and 6). Specifically either transition can occur with little change in the other parameter. For the purine nucleosides, some small adjustment in P is necessary when the anti to syn transition occurs while the sugar is in the C3′-endo conformation. Also, in all nucleosides, the anti to syn transition nearly always occurs through a high anti intermediate.

These calculations also show that potential energy methods alone are insufficient to properly parametrize energy functions. The rapid increase in the computation speed of modern computers has contributed to a growing trend toward the use of free energy method for developing force fields for molecular modeling problems.[48,49] Our results show that $V(P,\chi)$ adiabatic maps give misleading results for the pyrimidines. It is well-known that the syn conformation is rare in pyrimidines,[6,16,31] but Figures 7A and 8A show nearly identical energies for anti and syn. MD sampling of PMF(P,χ) conformational space, however, gives much more reasonable anti and syn distributions (Figures 7B and 8B). MD simulations also showed that ν_m contributes entropically to furanose flexibility. For example, repuckering activation energies in the O4′-endo and O4′-exo regions calculated from MD, (Figure 3) are lower than those calculated from adiabatic mapping (Figure 4), since ν_m is free during MD simulations. This is not readily apparent in potential energy calculations where it is necessary to constrain ν_m.

Admittedly, the behavior of free nucleosides will not be identical to that of nucleotide residues in a nucleic acid polymer. We contend, however, that even though individual residues in a nucleic acid may not have the same freedom of motion available to free nucleosides, qualitatively their potential surfaces will be the same. For example, C2′-endo and C3′-endo minima and anti and syn minima preferences are maintained in RNA and DNA. More important, accurate force fields for individual nucleotides are essential for accurate simulations on larger nucleic acids. It will be interesting to see how base stacking and sugar–phosphate backbone forces affect dN PMF(P,χ) surfaces.

Acknowledgment. Contributions to this work are S.C.H., who defined the initial problem, and H.A.G., who developed the necessary simulation and analysis programs, carried out and analyzed the simulations, and wrote the manuscript. The authors would like to thank Dr. Robert K.-Z. Tan for supplying some source code used in our molecular mechanics program, Dr. Bernard Brooks for supplying the Taylor expansion source code used to avoid singularities in improper torsion calculations,[41] and Mr. Michael McBride for his expert advice in Fortran programming. This work was supported by a grant to S.C.H. from the National Institutes of Health (GM-34015).

(48) Bell, C. D.; Harvey, S. C. *J. Phys. Chem.* **1986**, *90*, 6595–6597.
(49) Pearlman, D. A.; Kollman, P. A. *J. Am. Chem. Soc.* **1991**, *113*, 7167–7177.